Sustainable Environment Research 27 (2017) 70–76

Contents lists available at ScienceDirect

Sustainable Environment Research

journal homepage: www.journals.elsevier.com/sustainable-environment-research/

Original Research Article

Influence of carbon-functional groups with less hydrophilicity on a TiO_2 photocatalyst for removing low-level elemental mercury

Cheng-Yen Tsai [a], Yu-Tsai Pan [b], Yao-Hsuan Tseng [c], Chen-Wuing Liu [a], Tien-Ho Kuo [d], Hsing-Cheng Hsi [e,*]

[a] Department of Bioenvironmental Systems Engineering, National Taiwan University, Taipei 106, Taiwan
[b] Institute of Environmental Engineering and Management, National Taipei University of Technology, Taipei 106, Taiwan
[c] Department of Chemical Engineering, National Taiwan University of Science and Technology, Taipei 106, Taiwan
[d] Department of Environmental Engineering, Tungnan University, New Taipei City 222, Taiwan
[e] Graduate Institute of Environmental Engineering, National Taiwan University, Taipei 106, Taiwan

ARTICLE INFO

Article history:
Received 7 October 2016
Received in revised form
21 December 2016
Accepted 19 January 2017
Available online 25 January 2017

Keywords:
Carbon impregnation
Titanium dioxide
Elemental mercury
Photocatalysis
Competitive adsorption

ABSTRACT

A carbon-containing titanium dioxide (C-TiO_2) photocatalyst was prepared via ethanol impregnation using commercial Ishihara ST-01 TiO_2 powder as the precursor. Scanning Electron Microscopy and X-ray Diffractometry results indicated that raw ST-01 and C-TiO_2 had similarly globular shapes and presented in anatase phase. N_2 adsorption isotherms suggested that carbon impregnated on the TiO_2 surface could slightly reduce the total surface area and pore volume. X-ray Photoelectron Spectroscopy and Fourier Transform Infrared Spectroscopy examinations further supported the formation of various C-functional groups on the C-TiO_2 surface. Removal of low-concentration Hg^0 by raw and C-TiO_2 was enhanced with increasing O_2 concentration. Furthermore, because the existence of C-functional groups on the C-TiO_2 surface, the photoinduced hydrophilicity resulted from light irradiation appears to decrease, causing less adsorption competition from H_2O for Hg^0 adsorption at higher temperature. The reemission of adsorbed Hg species could thus be significantly decreased by carbon impregnation.

1. Introduction

Exhaust of mercury (Hg) through anthropogenic sources is a global issue due to its stability, bioaccumulation in ecosystems, and severe neurotoxic impacts on human health. Coal-fired power plants have been recognized a major source for significant Hg exhausts [1]. However, successful control of the low-level Hg (i.e., at 1–10 μg Nm^{-3} level) existing in the flue gases when coal is burned is difficult to achieve. Generally, elemental (Hg^0), oxidized (Hg^{2+}), and particle-bound (Hg_p) Hg are the three major Hg species in emission gases [2]. Several approaches have been employed to remove low-level Hg from combustion gas streams. Traditional air pollution control devices (APCDs), namely electrostatic precipitators and wet flue gas desulfurization, can readily remove Hg_p and Hg^{2+} from flue gases. Hg^0 is insoluble in water and highly volatile; therefore, it is scarcely controlled with the traditional APCDs.

Titanium dioxide (TiO_2) has been well demonstrated in terms of its excellent oxidative abilities in numerous environmental applications [3–6]. TiO_2 absorbs photons and generates active oxygen species (e.g., O_2^- ions and OH radicals) via reactions with O_2 and H_2O adsorbed on its surface [7]. These active oxygen species possess high oxidation potentials to decompose various contaminants in gaseous and aqueous phases [8,9]. Some researchers have reported that TiO_2 photocatalysis can be an innovative approach for Hg^0 oxidation and removal. For instance, others removed Hg from combustor exhaust by using titania particles irradiated with ultraviolet (UV) light [10,11]. Pitoniak et al. employed SiO_2–TiO_2 composites to remove Hg vapor under UV irradiation [12] and further suggested that both Hg^0 and Hg^{2+} were captured by the SiO_2–TiO_2 composites [13]. ACPDs can then subsequently capture the Hg-containing TiO_2 nanoparticles to achieve Hg abatement in gaseous phase [10].

* Corresponding author.
E-mail address: hchsi@ntu.edu.tw (H.-C. Hsi).
Peer review under responsibility of Chinese Institute of Environmental Engineering.

http://dx.doi.org/10.1016/j.serj.2017.01.003

In our previous works, Al- and Cu-doped TiO_2 nanoparticles were fabricated using a single-step method with the assistance of a non-transferred DC thermal plasma system [14,15]. Thermal plasma could provide sufficient energy to dope metal into the crystal structure of TiO_2, causing a substitution of metal for Ti instead of only physical deposition of metal onto the TiO_2 surface. Hg breakthrough tests indicated that the doped Cu in TiO_2 minimized desorption of Hg under high moisture condition [15]. However, the expensive and energy-consuming thermal plasma equipment limits its potential application on surface modification of photocatalysts from practical aspects. In contrast, aqueous-phase impregnation followed with low-temperature thermal treatment is more economically feasible and widely applied to alter the surface of photocatalyst nanomaterials.

One of the key findings in our previous studies was that humidity strongly inhibited the adsorption of Hg^0 resulting in a significant release of the adsorbed Hg species from the raw and surface-modified TiO_2 surface [15,16]. Therefore, to increase the adsorption of Hg^0, surface functional groups that can form a strong bond with Hg^0 (such as N-containing groups) [17] or can enhance the hydrophobicity of the TiO_2 surface limiting the competitive adsorption of Hg^0 from H_2O should be generated on the TiO_2 surface. A number of studies have reported the photocatalytic effectiveness of carbon (C)-doped and C-impregnated titania materials [18–24], in which the researchers proposed that carbonaceous species may act as sensitizers when UV or visible-light (VL) irradiates. One of these studies used *n*-hexane to modify anatase-phase titanium dioxide. The carbon deposition on the surface of TiO_2 formed $-CH_3$ (alkenes) groups, which reduced the extent of hydroxyl groups on the titanium dioxide surface, and as a result, altered the TiO_2 surface from hydrophilic to hydrophobic [25].

This research investigates the effectiveness of C-containing TiO_2 (C-TiO_2) on removal of low-level Hg^0 (i.e., in μg Nm^{-3} level). In our previous research, using thermal plasma fabricated Cu-TiO_2 with hydrophobic surface to inhibit competitive adsorption between H_2O and Hg^0 was successful but considered energy-inefficient. In contrast, in this study, a simple impregnation followed by low-temperature calcination was selected to introduce the C-functional groups onto the TiO_2 surface. The proposed C-impregnation method could lead to hydrophobic surface of TiO_2 for reducing competitive adsorption of Hg^0 from H_2O in a humid circumstance, which is well known to significantly decrease the Hg removal efficiency of TiO_2 even though low-level moisture is present. The Hg^0 removal effectiveness of raw and C-TiO_2 with the existence of O_2, H_2O, different light irradiation, and various test temperature was investigated and discussed. The presented work additionally focused on the hydrophobicity enhancement provided by the introduction of C-functional groups and the subsequent competitive adsorption effects of H_2O on Hg^0 removal. To the best of the authors' understanding, this is the first study to use C-impregnated TiO_2 for testing Hg^0 removal at μg Nm^{-3} level.

2. Experimental methods

2.1. Preparation of carbon-containing TiO_2 photocatalyst

C-containing TiO_2 nanoparticles were prepared via impregnation using anhydrous ethanol (CH_3CH_2OH) liquid as the carbon source and commercial titanium dioxide ST-01 (Ishihara Sangyo Kaisha, Japan), 100% anatase phase as the precursor. ST-01 TiO_2 powder of 10 g and 100 mL CH_3CH_2OH were initially mixed, and then it was agitated at 500 rpm for 1 h. The precipitated TiO_2 was dried in the hot plate at 70 °C and the dried powder was then calcined in air at 200 °C for 5 h. After calcination, the sample was cooled to room temperature and stored for characterization and Hg^0 removal experiments.

2.2. Characterization of raw and C-containing TiO_2 nanoparticles

The morphology of synthesized C-TiO_2 and raw ST-01 nanoparticles was analyzed using a transmission scanning electron microscope (SEM, Hitachi S-4800). Powder X-ray Diffractometry (XRD, PANalytical X'Pert PRO) with 45 kV accelerating voltage and 40 mA applied current was applied to identify the crystal structure. The scan range (2θ) of the XRD was set from 20° to 80° with a scanning rate of 0.02° s^{-1}. The crystalline phases were characterized with the database of the Joint Committee on Powder Diffraction Standards. Brunauer–Emmett–Teller (BET) specific surface area (S_{BET}) and total pore volume (V_{total}) were examined using a Quantachrome NOVA 2000 on the basis of the N_2 adsorption isotherms obtained at 77 K. The surface functional groups of raw and resulting samples were determined using X-ray photoelectron spectroscopy (XPS, VG Scientific ESCALAB 250) and a Fourier transform infrared spectrometer (FTIR, Excalibur series FTS-3500). The XPSPEAK® software was used to deconvolute the XPS data.

2.3. Hg adsorption/desorption tests

Raw ST-01 and the resulting C-TiO_2 samples were evaluated for their removal efficiency of low-level Hg^0. The experimental apparatus and methods resemble our previous researches [16,17]. The test equipment consists of key components including a photochemical reactor, a mixing gas generation portion, and a data acquisition system. Hg^0 was released from a certificated Hg^0 permeation tube (VICI Metronics) at 70 ± 0.1 °C to produce a constant Hg^0 diffusion concentration. The gas stream with known concentration of Hg^0 mixed with N_2, O_2, and water vapor was then generated with given moisture content. The mixing gas then flowed through a temperature-controlled reactor and heated Teflon tubes in which moisture condensation was prevented. Because the extremely low-concentration Hg^0 flue gas stream (i.e., < 10 μg Nm^{-3}) in a typical Taiwan coal-fired power plant is difficult to stably generate in our test system; in this study, Hg^0-containing gas with concentration of 15 ± 5 μg Nm^{-3} was prepared and flowed at a rate of 1.2 standard L min^{-1} passing the reactor which contained 5 mg of samples homogeneously distributed onto eight pieces of glass. The photochemical reactor was irradiated with UV or VL. The wavelength of UV lamp (F10T8BLB, Sankyo Denki) is 325–400 nm with a sharp peak exhibiting at 364.5 nm. A household halogen lamp (ESS-DE-500W, Philips) was applied as a VL source, which possessed a broad peak between 450 and 800 nm. Two different spectra (UV and VL) were verified through a spectrophotometer (Ocean Optics, USB2000). The photochemical reactor was irradiated by two UV lamps. The lamps were located at around 5 cm from the reactor; the UV intensity (3.5 ± 0.5 mW cm^{-2}) was identified by a Lutron YK35-UV light meter. Since the halogen VL lamp possessed strong light irradiation, the distance between the reactor and halogen lamp was about 40 cm to confirm the VL intensity at 3.8–4.5 mW cm^{-2} according to the Lutron LX-103 light meter. Because the VL lamp still emitted a certain UV (0.01–0.03 mW cm^{-2}), a thin polycarbonate plate UV filter was set between the VL lamp and reactor to avoid potential UV interference.

The Hg^0 removal experiments were carried out at three different temperatures and atmospheric pressure. Firstly, the photocatalytic reactions were performed at approximately 25 °C (i.e., room temperature). Elevating the experimental temperature, however, may further increase catalytic oxidation but decrease the adsorption of Hg species [16,17]. In order to clarify the effects of reaction

temperature, Hg removal experiments at 50 and 100 °C were also performed. The exhaust gas from the reactor passed through heated lines to an impinger containing 20% $SnCl_{2(aq)}$ which can transform any oxidized Hg compounds into Hg^0. And then, the gas passed through an impinger containing 12% $Na_2CO_{3(aq)}$ to ensure the gas acidic component free. Across the impinger, the gas passed a Nefion tube to remove H_2O to protect the downstream detector system. The exhaust gas from the impinger solution then flowed through a gold amalgamation system (Brooks Rand model AC-01) in which the gas phase Hg^0 was adsorbed. Hg^0 on the gold amalgam was then thermally desorbed (> 400 °C) and delivered as a concentrated gas-phase Hg^0 to a cold-vapor atomic fluorescence spectrophotometer (CVAFS; Brooks Rand Lab Model III) for analysis. Before the exhaust passed to the fume hood, all streams were flowed through a carbon trap. A test run used 6 min; each experimental condition was employed for 10 runs. The average Hg^0 removal efficiency (E_{cap}) of the total test runs was then determined as

$$E_{cap}(\%) = \frac{1}{n}\sum \frac{Hg^0_{in} - Hg_{T,out}}{Hg^0_{in}} \times 100 \quad (1)$$

where Hg^0_{in} represents the inlet Hg^0 concentration, $Hg_{T,out}$ denotes the outlet Hg concentration, which includes the original Hg^0 and the Hg^0 reduced from the photocatalytic Hg^{2+}, and n for here is 10 (runs). The blank test (without photocatalyst) of experimental equipment was also performed; the results demonstrated negligible Hg^0 removal for all experimental conditions.

3. Results and discussion

3.1. Physical and chemical properties of raw and C-containing TiO_2

The SEM images of the commercial ST-01 nanoparticles and the sample after carbon impregnation, designated as C-TiO_2, are shown in Fig. 1. Significant changes on the surface morphology and the particles size were not observed for the samples after carbon impregnation and calcination at 200 °C. The form of the synthesized samples was shown to be spherical and the nanoparticle size was approximately 20–30 nm.

Fig. 2 illustrates the XRD patterns of raw ST-01 and C-TiO_2 nanoparticles. The crystal phase of the resulting C-TiO_2 sample was similar to that of the raw ST-01. The peaks of XRD pattern for the (101), (004), (200), (105), and (211) reflect characteristics of the TiO_2 anatase phase appeared in raw and C-TiO_2. These experimental results suggest that the rutile phase is not generated during the impregnation process, mainly attributed to the low calcination temperature at 200 °C.

In contrast to particle size, morphology, and XRD patterns, changes in S_{BET} and V_{total} between raw ST-01 and C-TiO_2 were observed. The S_{BET} and V_{total} of the test sample decreased from 266 $m^2\ g^{-1}$ and 0.637 $cm^3\ g^{-1}$ for raw ST-01 to 246 $m^2\ g^{-1}$ and 0.624 $cm^3\ g^{-1}$ for C-TiO_2. Others also reported that a decrease in surface area while TiO_2 was modified by carbon impregnation [26,27]. The decrease in S_{BET} and V_{total} of the sample as a result of pore blockage may be caused due to the introduction of the carbon groups, generated from the anhydrous ethanol, deposited onto the TiO_2 surface. The decrease in surface area and pore volume may also stem from the slight growth of nanoparticles due to C impregnation.

The XPS spectra of C1s for the C-TiO_2 are shown in Fig. 3. Three XPS peaks at 284.9, 286.4, and 288.9 eV were deconvoluted from the C1s peak, representing the presence of adventitious elemental carbon (C–C), C–O/COR(H), and C=O, respectively [20,22–24,28,29]. The peaks of binding energy at 286.4 and 288.9 eV

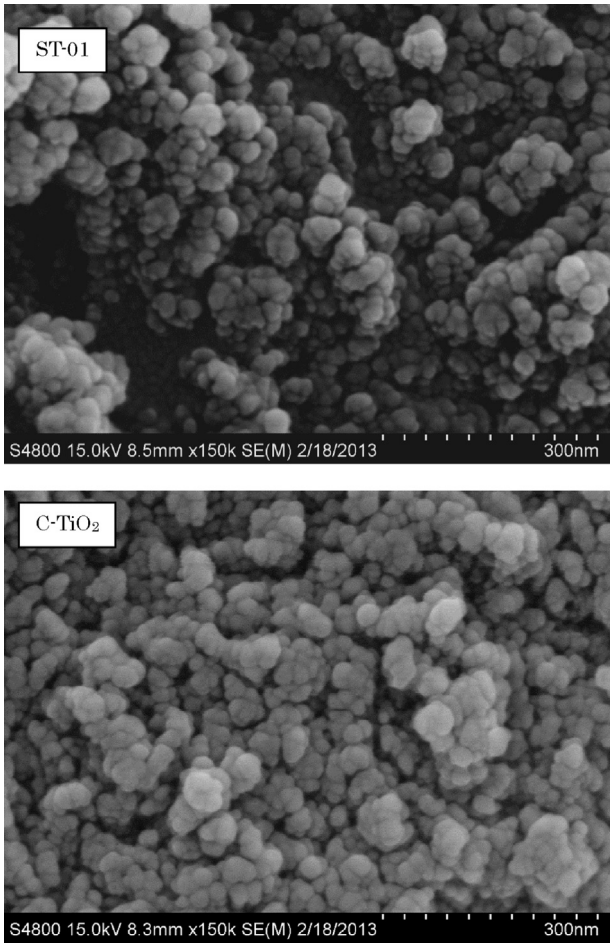

Fig. 1. SEM images of raw ST-01 and C-TiO_2 nanoparticles.

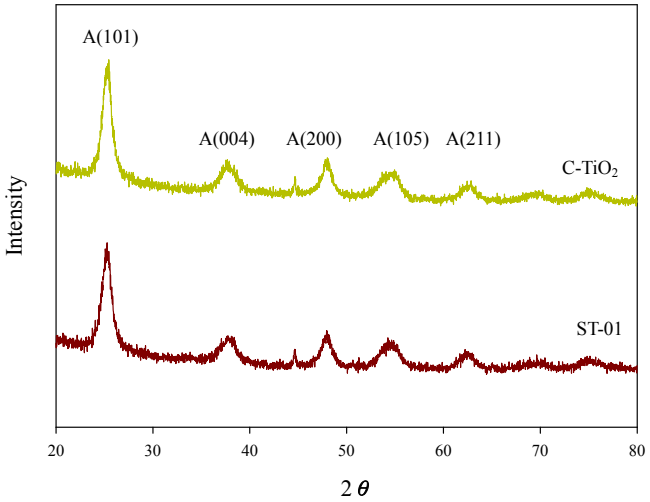

Fig. 2. XRD spectra of raw ST-01 and C-TiO_2.

corresponded to the oxidized carbon species from alcohol [30]. These results suggest that carbonaceous species such as a condensed and coke-like structure may exist on the surface of synthesized sample. These two peaks may also imply the presence of carbonate species in forms of an interstitial dopant [31]. Nevertheless, the formation of interstitial carbon during C-TiO_2 synthesis

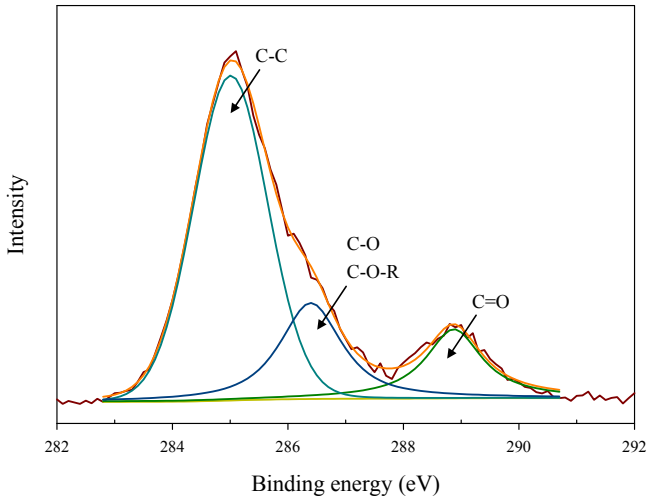

Fig. 3. The deconvolution of C1s XPS spectra for C-TiO_2 sample.

requires vast energy. Additionally, the Ti-C structure (binding energy at 281 eV) was not measured due to the temperate calcination condition as well. Therefore, the impregnation temperature at 200 °C in this study should not lead to the production of interstitial carbon.

FTIR was further applied to scrutinize the carbonaceous species on the synthesized C-TiO_2, as shown in Fig. 4. The FTIR analysis on raw ST-01 showed two peaks at 1635 and 2900–3800 cm^{-1}; the first peak stood for the OH group of ST-01 surface and the second broad peak corresponded to the surface adsorbed water molecules [32]. After carbon impregnation, two peculiarly broad peaks at 1434 and 1546 cm^{-1} shown in C-TiO_2 corresponded to the conglomeration of COOR, C–H, C=C, and C–O functional groups [32,33]. The foregoing functional groups can be attributed to acetate-like compounds [33]. The broad peaks at 1434 and 1546 cm^{-1} also corresponded to the deconvoluted results of binding energy peaks at 286.4 and 288.9 eV in the XPS spectra. Several metal and anionic atoms, including the carbonaceous species bound to TiO_2, have been shown to conduct e^- easily while the e^- was generated from the TiO_2 by irradiation; correspondingly, the C-containing titania may possess the lower efficiency for recombination of e^-/h^+ pairs [34–39].

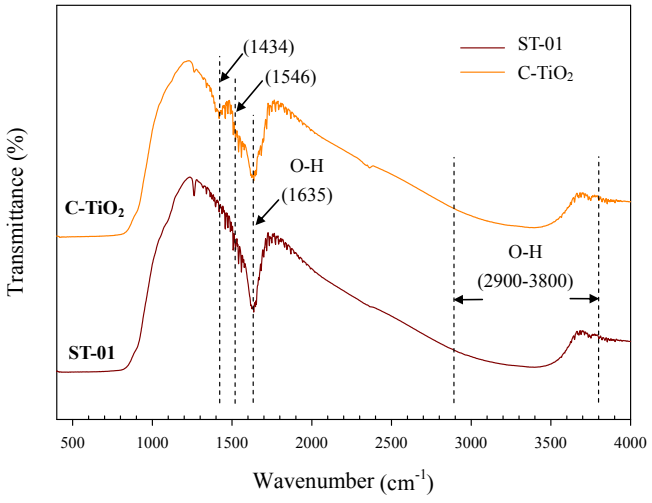

Fig. 4. FTIR spectra of raw ST-01 and C-TiO_2 photocatalysts.

3.2. Hg removal with raw and C-TiO_2 and discussion on adsorption/desorption mechanisms

Fig. 5 show the Hg adsorption and desorption dependence of raw ST-01 and C-TiO_2 nanoparticles on various test conditions, including the presence of humidity, various O_2 concentration, the type of light sources, and three different temperatures at 25, 50, and 100 °C. These conditions were alternately examined by gradually elevating the O_2 concentration from 0 to 6 and then to 21% combined with bringing in H_2O (approximately 25% relative humidity) and UV/VL irradiation to the photoreactor. The average Hg^0 removal efficiency (E_{cap}) of raw ST-01 and C-TiO_2 are further calculated and summarized in Tables 1 and 2 respectively for clarity. Firstly, tests were performed under dark condition with 0% O_2 and dry (i.e., moisture < 0.1 vol%) at 25 °C. It was observed that

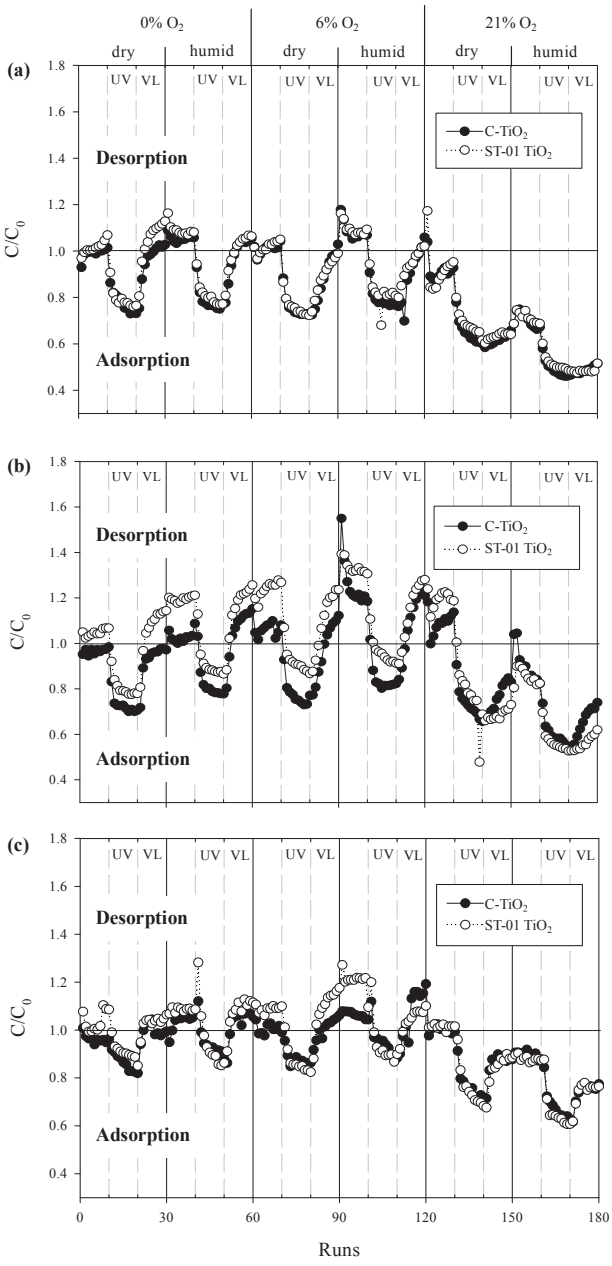

Fig. 5. Hg^0 breakthrough behaviors for ST-01 and C-TiO_2 nanoparticles at (a) 25 °C, (b) 50 °C, and (c) 100 °C.

Table 1
Average Hg removal efficiency (E_{cap} in %) for raw ST-01 TiO_2 sample at different test conditions ($n = 10$).

		Dark	UV	VL
25 °C	0% O_2-dry	−1.5 ± 2.8	20.6 ± 4.4	−4.2 ± 9.9
	6% O_2-dry	−1.8 ± 2.6	24.0 ± 4.4	11.0 ± 8.3
	21% O_2-dry	7.9 ± 9.9	31.5 ± 5.0	36.7 ± 1.4
	0% O_2-humid	−9.1 ± 2.7	18.8 ± 5.3	0.2 ± 8.3
	6% O_2-humid	−9.7 ± 3.0	18.2 ± 6.3	6.4 ± 7.2
	21% O_2-humid	28.9 ± 2.3	48.4 ± 3.5	51.5 ± 1.1
50 °C	0% O_2-dry	−4.8 ± 1.5	19.4 ± 4.5	−6.3 ± 10.5
	6% O_2-dry	−23.8 ± 3.7	7.9 ± 5.8	−10.4 ± 13.3
	21% O_2-dry	−19.5 ± 3.7	22.6 ± 13.5	31.4 ± 2.4
	0% O_2-humid	−19.6 ± 1.1	8.5 ± 8.0	−15.2 ± 11.7
	6% O_2-humid	−33.6 ± 3.1	3.8 ± 5.8	−14.1 ± 13.6
	21% O_2-humid	14.7 ± 3.5	43.2 ± 4.9	43.7 ± 3.3
100 °C	0% O_2-dry	−3.8 ± 4.5	9.1 ± 3.6	−3.2 ± 3.1
	6% O_2-dry	−8.9 ± 1.4	13.1 ± 5.7	−9.4 ± 8.8
	21% O_2-dry	−1.4 ± 1.0	24.2 ± 8.4	15.8 ± 6.7
	0% O_2-humid	−8.4 ± 1.0	4.9 ± 13.2	−7.6 ± 6.5
	6% O_2-humid	−20.6 ± 4.4	6.0 ± 9.7	−4.3 ± 5.3
	21% O_2-humid	11.8 ± 1.2	33.9 ± 8.2	25.9 ± 4.9

Table 2
Average Hg removal efficiency (E_{cap} in %) for C-TiO_2 sample at different test conditions ($n = 10$).

		Dark	UV	VL
25 °C	0% O_2-dry	0.8 ± 2.4	22.1 ± 4.5	3.8 ± 8.5
	6% O_2-dry	−0.9 ± 2.3	24.3 ± 4.9	11.5 ± 10.1
	21% O_2-dry	8.4 ± 4.7	35.0 ± 5.5	38.2 ± 2.3
	0% O_2-humid	−5.6 ± 1.5	21.2 ± 5.4	2.0 ± 9.5
	6% O_2-humid	−8.9 ± 3.8	20.7 ± 4.3	10.1 ± 11.9
	21% O_2-humid	29.9 ± 3.1	50.8 ± 3.8	51.6 ± 1.6
50 °C	0% O_2-dry	3.4 ± 1.3	27.2 ± 3.9	7.2 ± 7.9
	6% O_2-dry	−6.1 ± 2.7	22.3 ± 5.8	2.2 ± 12.7
	21% O_2-dry	−9.3 ± 5.2	26.4 ± 7.2	24.0 ± 7.0
	0% O_2-humid	−3.0 ± 2.6	17.6 ± 7.8	−5.9 ± 10.9
	6% O_2-humid	−26.3 ± 11.4	15.6 ± 6.5	−9.0 ± 14.3
	21% O_2-humid	9.6 ± 8.0	40.0 ± 5.5	34.8 ± 7.1
100 °C	0% O_2-dry	3.6 ± 1.8	13.7 ± 3.6	0.2 ± 3.1
	6% O_2-dry	−0.6 ± 2.2	12.2 ± 3.1	−0.7 ± 4.7
	21% O_2-dry	−0.4 ± 1.6	23.4 ± 5.9	13.9 ± 5.4
	0% O_2-humid	−3.7 ± 3.6	5.4 ± 6.8	−3.0 ± 6.5
	6% O_2-humid	−6.4 ± 1.3	5.1 ± 6.7	−7.7 ± 10.7
	21% O_2-humid	10.4 ± 1.5	31.8 ± 6.5	26.2 ± 4.7

fast Hg breakthrough (Runs 0–10 in Fig. 5a) occurred, indicating that most of Hg^0 immediately flowed through the photoreactor (E_{cap} was approximately −1.5% in raw ST-01 and 0.8% in C-TiO_2; Tables 1 and 2). This observation was expected and similar with our earlier works because the main Hg species at arid, O_2-free, and dark condition was Hg^0, under which a strong binding between Hg^0 and the TiO_2 surface was difficult to form [16,40]. In contrast, E_{cap} significantly increased to 20.6% for raw ST-01 (Table 1) and 22.1% for C-TiO_2 (Table 2) when UV started to irradiate (Runs 11–20 in Fig. 5a). These results indicate that both nanoparticles have greater photocatalytic potentials to transform Hg^0 into Hg^{2+} with their inherent surface-adsorbed oxygen. These test data also support that Hg^0 mainly heterogeneously reacts with the TiO_2 surface to form an adsorbed state, instead of homogeneously reacting with given gaseous components [16,41]. Although several researchers have reported that C-containing TiO_2 could induce VL absorption and response [18–24], in this study, VL irradiation showed minor effect on Hg^0 transformation into Hg^{2+} under 0% O_2 and arid condition for both TiO_2 nanoparticles as compared to the results from UV irradiation experiments (Runs 21–30 in Fig. 5a).

Moisture possessed marked effect on Hg^0 removal, which caused desorption of Hg from the raw ST-01 and C-TiO_2 surface, especially under the dark environment (i.e., Runs 31–40 in Fig. 5a; E_{cap} = −9.1% and −5.6% for raw ST-01 and C-TiO_2, respectively; Tables 1 and 2). These results support that Hg species and H_2O may compete for active sites on TiO_2 surface. Another earlier report also indicated that Hg^0 removal was influenced by the concentration of moisture [42].

The aforementioned data correspond to our earlier studies using oxygen-vacant TiO_2 and N-TiO_2 as the photocatalysts [16,17]. Fujishima et al. also reported the surface hydrophilicity of TiO_2 can be increased because of light irradiation [9]. The photocatalytic ability of TiO_2 may not be affected while H_2O existed in the gas stream; however, it markedly impacted the Hg removal by TiO_2. In this study, although the moisture content is at a low level of about 25% relative humidity, it is still much larger than the Hg^0 concentration (i.e., 15 ± 5 μg Nm^{-3}). Noting that E_{cap} = 21.2% for C-TiO_2 (Table 2) was larger than E_{cap} = 18.8% for raw ST-01 (Table 1) under the O_2-free condition (Runs 41–50 in Fig. 5a). These results indicate that the presence of C groups in TiO_2 reduces the H_2O adsorption and competition for active sites on TiO_2, as reported by Morawski et al. [25]. Even under VL irradiation, the E_{cap} of C-TiO_2 (2.0% in Table 2) was still slightly greater than the E_{cap} of ST-01 (0.2% in Table 1) by 1.79% (Runs 51–60 in Fig. 5a).

In contrast, increasing O_2 concentration enhanced the Hg^0 removal of C-TiO_2 nanoparticles (Runs 61–180 in Fig. 5a) due to the enhancement in catalytic oxidation of Hg^0. Notably, even under the dark condition, C-TiO_2 nanoparticles had significant Hg^0 removal to up to 29.9% when O_2 was at 21% (Runs 151–160 in Fig. 5a; Table 2). When light irradiated, the E_{cap} greatly enhanced to about 50.8% under UV and 51.6% under VL when O_2 was 21% (Runs 161–180 in Fig. 5a; Table 2), which indicates that Hg^0 oxidation and removal can be enhanced by light irradiation. The results support that Hg^0 is oxidized into Hg^{2+} in the presence of O_2 and consequently the Hg^0 removal efficiency is enhanced.

Fig. 5b and c shows the Hg^0 removal of raw ST-01 and C-TiO_2 at 50 and 100 °C, respectively with the corresponding E_{cap} listed in Tables 1 and 2. In general, Hg removal examined at raised temperature showed similar dependence on UV/VL irradiation, oxygen concentration, and existence of moisture with that obtained at 25 °C (Fig. 5a; Tables 1 and 2). Nevertheless, increasing temperature to 50 and 100 °C greatly decreased the Hg removal performance for raw ST-01 and C-TiO_2, supporting that the Hg species adsorption on the TiO_2 surface can be thermally desorbed due to its nature of exothermic adsorption [16,17]. It is also noticed that C-TiO_2 not only showed greater Hg adsorption than raw ST-01, but also encountered smaller adsorption competition from H_2O at elevating temperature (Fig. 5b and c; Tables 1 and 2). These results imply again that the C–OR(H), C=O, and C–O groups generated on the TiO_2 surface after carbon impregnation may also form stronger chemical bonds with Hg during higher temperature. Oxygen at 21% is still effective in enhancing Hg oxidation/adsorption at elevating temperature; however, the adsorption performance was smaller than that shown at 25 °C.

Based on the experimental results (Fig. 5b), C-functional groups on the C-TiO_2 surface appear to minimize desorption of Hg under high moisture condition. Li and Wu proposed comprehensive mechanisms on the capture and reemission of Hg^0 on the surface of TiO_2–SiO_2 nanocomposite [43]. The proposed mechanisms successfully explained the competitive adsorption between H_2O and Hg species due to the photoinduced superhydrophilicity of TiO_2 surfaces when UV was applied. By utilizing the concepts from Li and Wu as the foundation, the Hg^0 capture using C-TiO_2 under light irradiation is illustrated in Fig. 6. Under the 0% O_2 and arid condition (Fig. 6a), Hg^0 oxidation can only depend on the reactions via the slight content of O• and OH• radicals generated on the C-TiO_2 surface because of the pre-adsorbed O_2 and H_2O. Under the humid

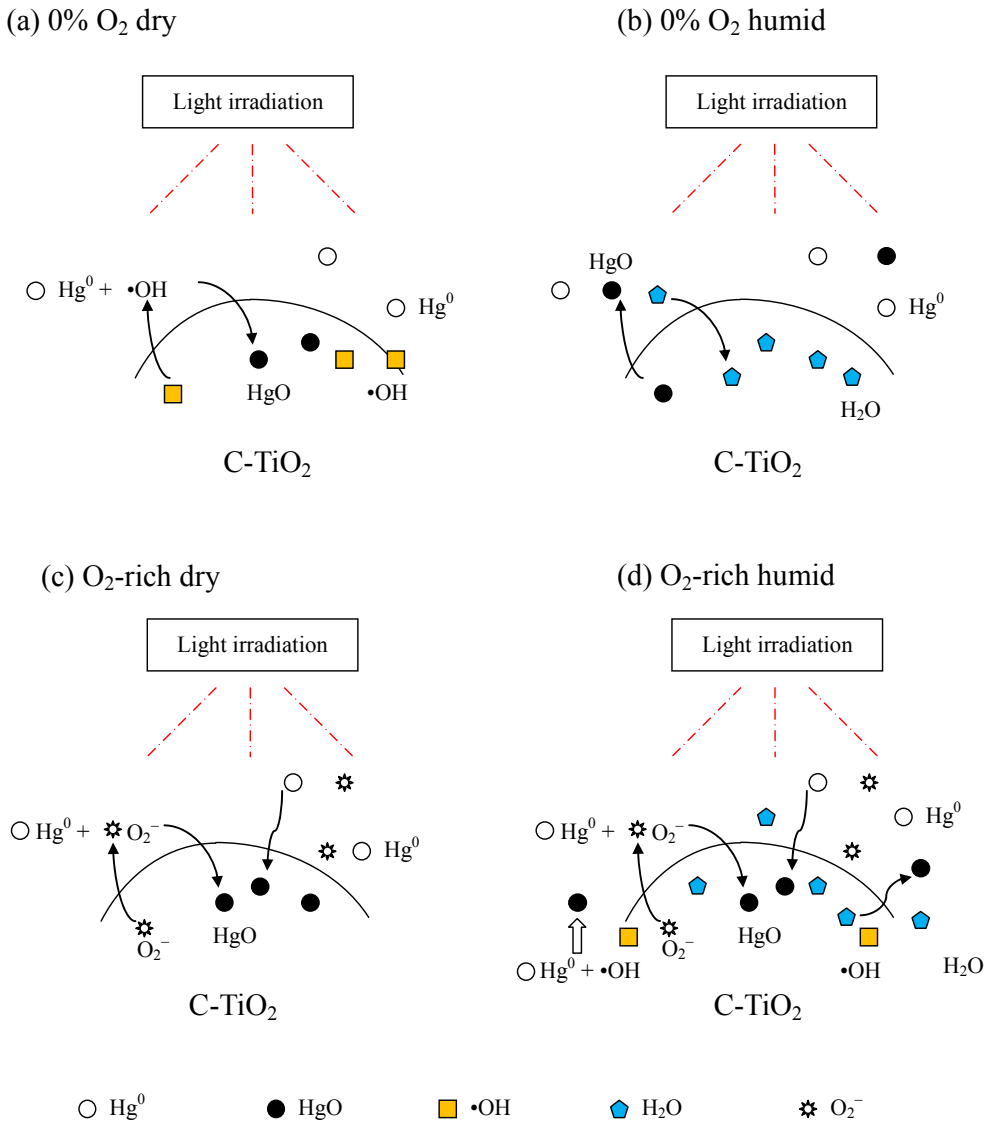

Fig. 6. Hypothetical mechanisms of Hg adsorption on and reemission from the surface of C-TiO_2 photocatalysts under visible light irradiation.

and 0% O_2 condition (Fig. 6b), H_2O molecules and Hg^0 will compete the active sites on the C-TiO_2 surface; therefore, leading to the reemission of formed HgO, which may subsequently reduce into Hg^0. Under the O_2-containing condition, Hg^0 oxidation is remarkably increased by elevating the O_2 concentration, but inhibited by H_2O molecule as the photoinduced superhydrophilicity of C-TiO_2 resulting in the H_2O competition adsorption (Fig. 6c and d). Results displayed here suggest that Hg species and C-TiO_2 maintain a weak bonding; consequently, it is reversible between the adsorbed Hg species and the C-TiO_2 surface.

For practical application, we suggest that the treated flue gas should contain sufficient O_2 to enhance the performance of the photoreactor with C-TiO_2 module, which is preferable to be aligned within the exhausting system as a fixed-bed reactor. Using air as carrier gas could be a feasible approach for Hg-containing tail gases, such as those from fluorescent lamp recycle plants. For flue gases from combustion sources such as coal-fired boilers, injection of C-TiO_2 nanoparticles followed by a particular matter collector can be used. Pretreatment pertaining to dehumidification before the exhaust gas flowed through the photoreactor is highly preferred to improve Hg^0 removal efficiency. The C-functional groups on the C-TiO_2 surface play an advantage role for inhibiting the photoinduced hydrophilicity of TiO_2 under light irradiation; consequently, the reemission of adsorbed Hg species could be reduced from the C-TiO_2 surface. It is also important to evaluate the lifetime and reuse potentials of C-TiO_2 for Hg removal in the next phase experiments for future pilot-plant and full-scale utilization.

4. Conclusions

C-containing TiO_2 photocatalyst was successfully prepared by a mild impregnation condition using ethanol as the carbon supplier. The impregnation temperature was 200 °C and samples were evidenced by SEM, XRD, BET, XPS, and FTIR. According to the SEM and XRD results, raw ST-01 and C-TiO_2 had similar morphology and crystal phases. The particle size was around 20–30 nm and both samples were in anatase phase. Nevertheless, C-TiO_2 had a slightly smaller BET surface area and total pore volume as compared to raw ST-01. C-functional groups including C–C, C–O/COR(H), and C=O were found on C-TiO_2 surface by XPS and FTIR examination. Under an O_2–free and dark condition, the Hg removal efficiency of C-TiO_2 was small; however, Hg removal efficiency was greatly increased by

elevating the O_2 concentration when light irradiated. The test results indicate that photocatalytic oxidation, namely Hg^0 transformation into Hg^{2+}, could be a deciding process to enhance the adsorption on Hg species onto the C-TiO_2 surface. H_2O exhibited deteriorating effects because the competition for active sites on the C-TiO_2 surface between Hg and H_2O molecule. Nevertheless, the decrease in surface hydrophilicity of C-TiO_2 when light irradiation, causing the observed reemission of adsorbed Hg species, can be greatly inhibited via carbon impregnation.

Acknowledgement

This work was partly supported by Ministry of Science and Technology, Taiwan (MOST 103-2313-B-002-018-MY3).

References

[1] Pacyna EG, Pacyna JM, Sundseth K, Munthe J, Kindbom K, Wilson S, et al. Global emission of mercury to the atmosphere from anthropogenic sources in 2005 and projections to 2020. Atmos Environ 2010;44:2487–99.
[2] Hsi HC, Lee HH, Hwang JF, Chen W. Mercury speciation and distribution in a 660-megawatt utility boiler in Taiwan firing bituminous coals. J Air Waste Manag 2010;60:514–22.
[3] Mattle MJ, Thampi KR. Photocatalytic degradation of Remazol Brilliant Blue® by sol-gel derived carbon-doped TiO_2. Appl Catal B Environ 2013;140–141:348–55.
[4] Wu X, Yin S, Dong Q, Guo C, Li H, Kimura T, et al. Synthesis of high visible light active carbon doped TiO_2 photocatalyst by facile calcinations assisted solvothermal method. Appl Catal B Environ 2013;142–143:450–7.
[5] Lyu J, Zhu L, Burda C. Considerations to improve adsorption and photocatalysis of low concentration air pollutants on TiO_2. Catal Today 2014;225:24–33.
[6] Sivachandiran L, Thevenet F, Gravejat P, Rousseau A. Isopropanol saturated TiO_2 surface regeneration by non-thermal plasma: influence of air relative humidity. Chem Eng J 2013;214:17–26.
[7] Fujishima A, Honda K. Electrochemical photolysis of water at a semiconductor electrode. Nature 1972;238:37–8.
[8] Hoffmann MR, Martin ST, Choi W, Bahnemann DW. Environmental applications of semiconductor photocatalysis. Chem Rev 1995;95:69–96.
[9] Fujishima A, Rao TN, Tryk DA. Titanium dioxide photocatalysis. J Photochem Photobiol C 2000;1:1–21.
[10] Wu CY, Lee TG, Tyree G, Arar E, Biswas P. Capture of mercury in combustion systems by *in situ*-generated titania particles with UV irradiation. Environ Eng Sci 1998;15:137–48.
[11] Lee TG, Biswas P, Hedrick E. Overall kinetics of heterogeneous elemental mercury reactions on TiO_2 sorbent particles with UV irradiation. Ind Eng Chem Res 2004;43:1411–7.
[12] Pitoniak E, Wu CY, Londeree D, Mazyck D, Bonzongo JC, Powers K, et al. Nanostructured silica-gel doped with TiO_2 for mercury vapor control. J Nanopart Res 2003;5:281–92.
[13] Pitoniak E, Wu CY, Mazyck DW, Powers KW, Sigmund W. Adsorption enhancement mechanisms of silica-titania nanocomposites for elemental mercury vapor removal. Environ Sci Technol 2005;39:1269–74.
[14] Tsai CY, Kuo TH, Hsi HC. Fabrication of Al-doped TiO_2 visible-light photocatalyst for low-concentration mercury removal. Int J Photoenergy 2012;2012:8.
[15] Tsai CY, Hsi HC, Kuo TH, Chang YM, Liou JH. Preparation of Cu-doped TiO_2 photocatalyst with thermal plasma torch for low-concentration mercury removal. Aerosol Air Qual Res 2013;13:639–48.
[16] Hsi HC, Tsai CY. Synthesis of TiO_{2-x} visible-light photocatalyst using N_2/Ar/He thermal plasma for low-concentration elemental mercury removal. Chem Eng J 2012;191:378–85.
[17] Chen SS, Hsi HC, Nian SH, Chiu CH. Synthesis of N-doped TiO_2 photocatalyst for low-concentration elemental mercury removal under various gas conditions. Appl Catal B Environ 2014;160–161:558–65.
[18] Khan SUM, Al-Shahry M, Ingler Jr WB. Efficient photochemical water splitting by a chemically modified n-TiO_2. Science 2002;297:2243–5.
[19] Lin YM, Tseng YH, Huang JH, Chao CC, Chen CC, Wang I. Photocatalytic activity for degradation of nitrogen oxides over visible light responsive titania-based photocatalysts. Environ Sci Technol 2006;40:1616–21.
[20] Tseng YH, Kuo CS, Huang CH, Li YY, Chou PW, Cheng CL, et al. Visible-light-responsive nano-TiO_2 with mixed crystal lattice and its photocatalytic activity. Nanotechnology 2006;17:2490–7.
[21] Hsu SW, Yang TS, Chen TK, Wong MS. Ion-assisted electron-beam evaporation of carbon-doped titanium oxide films as visible-light photocatalyst. Thin Solid Films 2007;515:3521–6.
[22] Kuo CS, Tseng YH, Huang CH, Li YY. Carbon-containing nano-titania prepared by chemical vapor deposition and its visible-light-responsive photocatalytic activity. J Mol Catal A-Chem 2007;270:93–100.
[23] Treschev SY, Chou PW, Tseng YH, Wang JB, Perevedentseva EV, Cheng CL. Photoactivities of the visible-light-activated mixed-phase carbon-containing titanium dioxide: the effect of carbon incorporation. Appl Catal B Environ 2008;79:8–16.
[24] Zabek P, Eberl J, Kisch H. On the origin of visible light activity in carbon-modified titania. Photoch Photobio Sci 2009;8:264–9.
[25] Morawski AW, Janus M, Tryba B, Inagaki M, Kałucki K. TiO_2-anatase modified by carbon as the photocatalyst under visible light. C R Chim 2006;9:800–5.
[26] Janus M, Kusiak E, Morawski AW. Carbon modified TiO_2 photocatalyst with enhanced adsorptivity for dyes from water. Catal Lett 2009;131:506–11.
[27] He Z, Que W, Chen J, He Y, Wang G. Surface chemical analysis on the carbon-doped mesoporous TiO_2 photocatalysts after post-thermal treatment: XPS and FTIR characterization. J Phys Chem Solids 2013;74:924–8.
[28] Sakthivel S, Kisch H. Daylight photocatalysis by carbon-modified titanium dioxide. Angew Chem Int Ed 2003;42:4908–11.
[29] Konstantinova EA, Kokorin AI, Sakthivel S, Kisch H, Lips K. Carbon-doped titanium dioxide: visible light photocatalysis and EPR investigation. Chimia 2007;61:810–4.
[30] Janus M, Tryba B, Inagaki M, Morawski AW. New preparation of a carbon-TiO_2 photocatalyst by carbonization of n-hexane deposited on TiO_2. Appl Catal B Environ 2004;52:61–7.
[31] Fu R, Yoshizawa N, Dresselhaus MS, Dresselhaus G, Satcher JH, Baumann TF. XPS study of copper-doped carbon aerogels. Langmuir 2002;18:10100–4.
[32] Huang Y, Ho W, Lee S, Zhang L, Li G, Yu JC. Effect of carbon doping on the mesoporous structure of nanocrystalline titanium dioxide and its solar-light-driven photocatalytic degradation of NO_x. Langmuir 2008;24:3510–6.
[33] Kang IC, Zhang Q, Yin S, Sato T, Saito F. Preparation of a visible sensitive carbon doped TiO_2 photo-catalyst by grinding TiO_2 with ethanol and heating treatment. Appl Catal B Environ 2008;80:81–7.
[34] Yu Y, Yu JC, Chan CY, Che YK, Zhao JC, Ding L, et al. Enhancement of adsorption and photocatalytic activity of TiO_2 by using carbon nanotubes for the treatment of azo dye. Appl Catal B Environ 2005;61:1–11.
[35] Jing L, Qu Y, Wang B, Li S, Jiang B, Yang L, et al. Review of photoluminescence performance of nano-sized semiconductor materials and its relationships with photocatalytic activity. Sol Energy Mater Sol C 2006;90:1773–87.
[36] Yu C, Yu JC. A simple way to prepare C–N-Codoped TiO_2 photocatalyst with visible-light activity. Catal Lett 2009;129:462.
[37] Elahifard MR, Rahimnejad S, Haghighi S, Gholami MR. Apatite-coated Ag/AgBr/TiO_2 visible-light photocatalyst for destruction of bacteria. J Am Chem Soc 2007;129:9552–3.
[38] Kowalska E, Abe R, Ohtani B. Visible light-induced photocatalytic reaction of gold-modified titanium (IV) oxide particles: action spectrum analysis. Chem Commun 2009;2:241–3.
[39] Tseng YH, Kuo CH. Photocatalytic degradation of dye and NO_x using visible-light-responsive carbon-containing TiO_2. Catal Today 2011;174:114–20.
[40] Tsai CY, Hsi HC, Bai H, Fan KS, Chen C. TiO_{2-x} nanoparticles synthesized using He/Ar thermal plasma and their effectiveness on low-concentration mercury vapor removal. J Nanopart Res 2011;13:4739–48.
[41] Presto AA, Granite EJ. Survey of catalysts for oxidation of mercury in flue gas. Environ Sci Technol 2006;40:5601–9.
[42] Li Y, Murphy P, Wu CY. Removal of elemental mercury from simulated coal-combustion flue gas using a SiO_2-TiO_2 nanocomposite. Fuel Process Technol 2008;89:567–73.
[43] Li Y, Wu CY. Role of moisture in adsorption, photocatalytic oxidation, and reemission of elemental mercury on a SiO_2-TiO_2 nanocomposite. Environ Sci Technol 2006;40:6444–8.